Pergamon

Acta Materialia 50 (2002) 4379–4394

Acta MATERIALIA

www.actamat-journals.com

# On the dependence of in-grain subdivision and deformation texture of aluminum on grain interaction

D. Raabe [a,*], Z. Zhao [a], W. Mao [b]

[a] *Max-Planck-Institut für Eisenforschung, Department for Microstructure Physics and Metal Forming, Max-Planck-Str. 1, 40237 Düsseldorf, Germany*

[b] *University of Science and Technology Beijing, Department of Materials Science and Engineering, 100083 Beijing, China*

Received 30 April 2002; received in revised form 23 June 2002; accepted 2 July 2002

**Abstract**

We present plane strain simulations about the dependence of orientational in-grain subdivision and crystallographic deformation textures in aluminum polycrystals on grain interaction. The predictions are compared to experiments. For the simulations we use a crystal plasticity finite element and different polycrystal homogenization models. One set of finite element simulations is conducted by statistically varying the arrangement of the grains in a polycrystal. Each grain contains 8 integration points and has different neighbor grains in each simulation. The reorientation paths of the 8 integration points in each grain are sampled for the different polycrystal arrangements. For quantifying the influence of the grain neighborhood on subdivision and texture we use a mean orientation concept for the calculation of the orientation spread among the 8 originally identical in-grain orientation points after plastic straining. The results are compared to Taylor–Bishop–Hill-type and Sachs-type models which consider grain interaction on a statistical basis. The study reveals five important points about grain interaction. First, the consideration of local grain neighborhood has a significant influence on the reorientation of a grain (up to 20% in terms of its end orientation and its orientation density), but its own initial orientation is more important for its reorientation behavior than its grain neighborhood. Second, the sharpness of the deformation texture is affected by grain interaction leading to an overall weaker texture when compared to results obtained without interaction. Third, the in-grain subdivision of formerly homogeneous grains occurring during straining is strongly dependent on their initial orientation. For instance some crystals build up in-grain orientation changes of more than 20° after 95% straining while others do practically not subdivide. Fourth, the dependence of in-grain subdivision on the neighbor grains is different for crystals with different initial orientation (cube or rotated Goss grains reveal strong subdivision). Fifth, the upper bound for the variation of texture due to changes in grain neighborhood amounts at most to 5% in terms of the positions of the main texture components. In terms of the overall orientation density all predictions (using different neighborhood configurations) remain within a narrow tube with an orientation scatter of 10% (β-fiber) to 20% (Brass component, α-fiber)) when the neighborhood changes. 

*Keywords:* Texture; Theory & modeling—structural behavior; Mechanical properties—plastic; Metals—crystalline; Mesostructure


PII: S1359-6454(02)00276-8

## 1. Introduction and motivation

Plastic straining of polycrystals entails crystalline orientation changes and the development of grain orientation distributions which are also referred to as crystallographic textures. Deformation textures are characteristic for the strained type of material, the inherited microstructure, and the macro- and micromechanical boundary conditions. Crystallographic orientation changes occur at different microstructural scales since initially uniformly orientated crystals do as a rule not rotate as units (macroscale or global texture formation) but can subdivide into portions with a range of different orientations within their original grain borders (microscale texture formation). The activation of plastic slip and hence also the spin arising from it are strongly dependent on the relationship between the crystallographic coordinate system and the external reference system created by the loading conditions (orientation). Consequently, texture evolution is at the micro- and macroscale a pronounced function of the starting texture. The present study addresses the evolution of crystallographic deformation textures at the grain- and subgrain scale in face centered cubic (fcc) polycrystals using aluminum as example. It places particular attention on the influence of the interaction of neighboring grains on the overall texture evolution and on in-grain orientation subdivision phenomena as well as on the comparison of crystal plasticity simulations with grain-interaction homogenization models.

We have four major motivations to tackle these questions. First, it is our aim to basically understand not only the mere dependence of subgrain and global texture formation on the grain neighborhood but to quantify the effects and derive their orientation dependence. Second, we want to understand the dependence of texture formation on grain neighborhood in order to validate existing phenomenological grain interaction approaches which are embedded in polycrystal homogenization models. Third, we consider it important to elucidate the orientation- and neighborhood dependence of the in-grain subdivision tendency with respect to the orientation dependence of the kinetic instability criterion of recrystallization nucleation. Fourth, we wish to identify the upper bound for the influence of grain interaction on texture evolution for better separating grain interaction effects from constitutive, i.e. grain-scale strain hardening effects, on the development of deformation textures.

These motivations require some remarks. Our first set of comments addresses the importance of the basic understanding of these texture phenomena. It is an important experimental observation, particularly since the introduction of advanced automated local orientation imaging techniques via interpretation of Kikuchi-diagrams obtained in the transmission- and scanning electron microscope, that texture development and in particular the orientation subdivision of originally uniform grains during loading depends on both, the initial orientation of a grain and on the grain neighborhood [1–9]. Although some experiments seem to suggest that the size of in-grain dislocation cell structures (but not their in-grain orientation distributions) can be scaled to one common master distribution, it are some of the most relevant texture components who are known to not coincide with this scaling. Furthermore, the scaling of in-grain dislocation cell sizes does not justify the conclusion of an equivalent scaling of the in-grain orientation distribution of the cells. Another aspect in this context is to better understand existing experimental and theoretical observations of the macro- and microscale texture evolution with respect to the clear separation of intrinsic effects (orientation dependence) and extrinsic effects (neighborhood dependence). As intrinsic effects we understand in this context the mere dependence of deformation texture phenomena on the orientation of the initial grain. For instance the micromechanics and the plastic spin of some orientations (say under plane strain loading) are so much governed by the activation of a small but dominating set of slip systems that minor changes in the micromechanical boundary conditions (e.g. different neighborhood) do not substantially alter the orientation change or the subdivision behavior. A typical example is the

* Corresponding author. Tel.: +49-211-6792-278; fax: +49-211-6792-333.
*E-mail address:* raabe@mpie.de (D. Raabe).

enormous micromechanical stability of the 45° about the normal rotated cube orientation $\{001\} < 110 >$ in body centered cubic (bcc) metals under plane strain conditions[1]. As extrinsic effects we understand in this context the dependence of deformation texture phenomena on the grain neighborhood and, more general, on the micromechanical boundary conditions. A strong extrinsic influence on the macro- and microtexture is particularly typical of instable orientations, for which minor changes in the boundary conditions entail different sets of activated slips and as a consequence a variety of plastic spins within the same original grain borders. A typical example is the cube component in fcc metals or the Goss component in bcc metals under plain strain loading. While the intrinsic origin of in-grain subdivision was recently discussed in terms of the orientation dependence of the divergence of the reorientation fields [10] the extrinsic influence on texture evolution is up to now less well understood.

Our second set of comments addresses the incorporation of neighborhood effects on texture and on grain subdivision into polycrystal homogenization models. These are approaches which use simplified external and internal boundary conditions to predict the elastic-plastic response of polycrystalline and multiphase materials at the meso- and macroscale without the explicit incorporation of the elastic–plastic interaction of neighboring grains or in-grain subdivision phenomena [see overviews in 11-15]. Polycrystal homogenization models replace real microstructures by simplified model ingredients. For instance the dynamics of intricate dislocation ensembles are essentially condensed into phenomenological hardening laws and crystallographic kinematics. The influence of the grain shape and size is typically reduced to micromechanical degrees of freedom with respect to the relaxation of certain strain rate constraints. The elastic–plastic co-deformation (not the true interaction) of the grains is mapped via strain rate homogenization (Taylor–Bishop–Hill-based approaches [16,17]), stress homogenization (Sachs-based approaches [18]), or the interaction between each grain and an average surrounding medium with the kinematic properties of the entire sample (self-consistent Eshelby–Kröner-based approaches [19–21]). Although polycrystal homogenization models hence obviously reduce the complexity of polycrystalline matter in a rather drastic fashion they still seem to capture some of the essential ingredients which govern polycrystal plasticity, particularly at large strains. This is evident by the astonishing qualitative accord between many polycrystal homogenization simulations and experiments as well as by the success of many yield surface and subsequent shape change predictions obtained by polycrystal models when incorporated in the form of anisotropic yield functions into otherwise microstructure-independent finite element formulations. Particularly the latter aspect is rapidly gaining momentum for efforts to derive physically based yield surface approximations from crystallographic textures and integrate them into finite element formulations for time-efficient industry-scale simulations of plastic forming operations [e.g. 22-27]. An important aspect of homogenization models in this context is to obtain quantitative results. Another important goal of current polycrystal homogenization models is to merge strain hardening theory and yield surface concepts. The aim of such efforts is to obtain a unified more-dimensional theory of the yield curve or—in other words—a dislocation dynamics based theory of the yield locus. The above aspects substantiate that polycrystal homogenization models play an important role in the field of polycrystal plasticity simulations, particularly with respect to engineering applications. Therefore, different approaches have been suggested in the past decades to render the classical Taylor–Bishop–Hill or Sachs homogenization models physically more plausible and in better accord with experimental data. Conceptual modifications of the constitutive descriptions consist essentially in the introduction of grain-interaction or respectively interaction penalty measures. These terms quantify the elastic–plastic mismatch between neighboring grains or within larger grain clusters where the interacting grains are typically selected statistically from a large set of single orientations (1000–5000) which

[1] The Miller indices of a crystal orientation {hkl}<uvw> indicate its crystallographic plane parallel to the sheet surface, {hkl}, and the crystallographic axis parallel to the longitudinal direction, <uvw>, assuming orthothropic sample symmetry.

map the inherited texture [28–31]. The real neighborhood arrangement of the grains is usually not accounted for, due to obvious reasons. An important point in this context is the question how realistic, necessary, and effective the respective grain interaction concepts are which are used in the different homogenization models. Another important feature still not grasped so far by these improved grain interaction homogenization models is that during deformation grains break up on a micrometer scale into deformation structures with different crystallographic orientation. Therefore, this study aims to answer the questions how important the influence of the neighborhood grain arrangement is on the global deformation textures and on the in-grain subdivision.

Our third set of comments addresses the importance of the orientation- and neighborhood dependence of in-grain subdivision phenomena with respect to the orientation dependence of the kinetic instability criterion of recrystallization nucleation. The phenomenological theory of primary static recrystallization states that nucleation can only take place in areas with large stored elastic energy (thermodynamic instability criterion) and large orientation gradients (kinetic instability criterion) (e.g. [32]). The latter point implies, that during discontinuous subgrain coarsening (in grains with high stacking fault energy) subgrains which rapidly accumulate large misorientations beyond the small-angle regime have a higher chance to act as discontinuous nuclei in the further course of recrystallization. This means that recrystallization nucleation must be considered as a problem which highly depends on the deformed host orientation in which it takes place.

Our fourth set of comments addresses the aim to identify the bounds for the influence of grain interaction on texture evolution. The various grain interaction approaches used by the improved homogenization models [28–31,33] and the comparison of their predictions with experimental data do alone not allow one to separate grain interaction effects from constitutive, i.e. grain-scale strain hardening effects on the texture development. It is up to now not completely understood which of the observed texture effects stem from the intrinsic orientation dependence of strain hardening or grain size effects and which stem from grain interaction phenomena.

The organization of the paper is as follows: The second section is about the experimental procedure. The third section describes the presentation of fcc textures. The fourth section describes the simulation procedures. In the fifth section the simulation results are discussed and compared to our own experimental data and to observations made by other groups.

## 2. Experiments

An aluminum sample with commercial purity (99.9 mass% Al) was chosen for comparing the various texture predictions with experimental results. At first a block of the aluminum sample was forged in three mutually perpendicular directions several times with gradually decreasing thickness reductions. This initial forming procedure was conducted in order to produce a fine grained microstructure with a random orientation distribution. From the previous literature on experimental rolling textures of aluminum it is well known that the generation of a random starting texture is very difficult, but it is an essential precondition for comparing texture predictions with experimental data. After forging the sample was cold rolled to 95% thickness reduction (expressed in terms of the engineering strain $\Delta d/d$, where $d$ is the initial sheet thickness). The textures were quantitatively examined by measuring the four incomplete pole figures {111}, {200}, {220}, and {113} in the range of the pole distance angle $\alpha$ from 5° to 85° using $Cu_{K\alpha 1}$ radiation. The measurements were carried out using a Bragg-type back-reflection set-up. From the experimental pole figures the orientation distribution function $f(g)$ was derived by use of the series expansion method ($1_{max} = 22$) and subsequently ghost corrected by use of spherical Gauss model functions.

## 3. Presentation of textures

Owing to the high symmetry of both the fcc crystal system and the orthorhombic sample sys-

tem which is set up by the rolling direction, RD, normal direction, ND, and transverse direction, TD, the rolling textures are presented in the reduced Euler space where an orientation is given by the three Euler angles $\varphi_1$, $\phi$, and $\varphi_2$ ($0° \leq \varphi_1, \phi, \varphi_2 \leq 90°$). Crystal orientations can also be conveniently described by use of Miller indices {hkl}<uvw>. In this concept the triple {hkl} describes the crystallographic plane which is parallel to the sheet surface whereas <uvw> indicates the direction parallel to the rolling direction. Since fcc metals usually tend to develop fiber type textures during rolling and plane strain compression, it is advantageous to also depict the orientation density by use of fiber diagrams. For further comparison we therefore use the α-fiber and the β-skeleton line [34]. Texture fibers are sections of an orientation distribution function which present the orientation density along one of the Euler angles where the other two angles remain constant. Crystallographically this presentation shows the change in orientation density for a rotation about a fixed crystal axis. A texture skeleton line is a special kind of texture fiber. It comprises the orientation density of three major texture components with variable coordinates in orientation space. This presentation is important when the inspected texture components are less symmetric and therefore not exactly located at a certain point in orientation space. This means a texture skeleton line always consists of two sets of information, namely, of the orientation density plot and of the coordinate plot in Euler space. For presenting textures of deformed aluminum the most important presentations are the $\alpha_{fcc}$-fiber which comprises all orientations with a common crystallographic fiber axis $< 011 >$ parallel to the normal direction including major components $\{011\} < 100 >$ (Goss-component, $\varphi_1 = 0°, \phi = 45°, \varphi_2 = 0°$), $\{011\} < 211 >$ (Brass-component, $\varphi_1 = 35°, \phi = 45°, \varphi_2 = 0°$), $\{011\} < 111 >$, and $\{011\} < 011 >$ (90° about the normal rotated Goss-component, $\varphi_1 = 90°, \phi = 45°, \varphi_2 = 0°$) and the less symmetric β-skeleton line including major components $\{211\} < 111 >$ (Copper-component, $\varphi_1 = 90°, \phi = 35°, \varphi_2 = 45°$), $\sim \{123\} < 634 >$ (S-component, $\varphi_1 = 60°, \phi = 32°, \varphi_2 = 65°$), and the Brass component $\{011\} < 211 >$.

## 4. Applied texture simulation methods

### *4.1. Basic constitutive model for the finite element simulations*

In the large-strain constitutive crystal plasticity model [35] used in the present work one assumes the stress response at each macroscopic continuum material point to be potentially given by one crystal or by a volume-averaged response of a set of grains comprising the respective material point. The latter assumption can be referred to as a local Taylor-type or local strain-rate homogenization assumption. In case of a multi-grain description the volume averaged stress amounts to

$$\langle \mathrm{T} \rangle = \sum_{k=1}^{N} (w_k \mathrm{T}_k) \tag{1}$$

where $N$ is the total number of individual orientations mapped onto an integration point using the Taylor assumption, $w_k$ the volume fraction of each single orientation, $\mathbf{T}_k$ the Cauchy stress produced by the $k$th individual orientation, and $\langle \mathbf{T} \rangle$ the volume average stress produced by all orientation mapped at the integration point. The constitutive equation for the stress in each grain is then expressed in terms of

$$\mathbf{T}^* = \mathbf{C}\mathbf{E}* \tag{2}$$

where $\mathbf{C}$ is the fourth order elastic tensor and $\mathbf{E}*$ an elastic strain measure obtained by polar decomposition,

$$\mathrm{E}^* = \frac{1}{2}(\mathrm{F}^{*\mathbf{T}}\mathrm{F}^* - 1) \tag{3}$$

which leads to a stress measure which is the elastic work conjugate to the strain measure $\mathbf{E}*$,

$$\mathrm{T}^* = \mathrm{F}^{*\text{-}1}(\mathbf{det}(\mathrm{F}^*)\mathrm{T})(\mathrm{F}^*)^{-\mathbf{T}} \tag{4}$$

where $\mathbf{T}$ is the symmetric Cauchy stress tensor in the grain, and $\mathbf{F}*$ is a local elastic deformation gradient defined in terms of the local total deformation gradient $\mathbf{F}$ and the local plastic deformation gradient $\mathbf{F}^P$. The relation between the elastic and the plastic portion of $\mathbf{F}$ amounts to

$$\mathrm{F}^* = \mathrm{F}(\mathrm{F}^{\mathbf{P}})^{-1} \quad , \quad \mathbf{det}(\mathrm{F}^*) > 0 \quad , \quad \mathbf{det}(\mathrm{F}^{\mathbf{P}}) = 1 \tag{5}$$

The plastic deformation gradient is given by the flow rule

$$\dot{\mathbf{F}}^{\mathbf{P}} = \mathbf{L}^{\mathbf{P}}\mathbf{F}^{\mathbf{P}} \tag{6}$$

with its crystalline portion

$$\mathbf{L}^{\mathbf{P}} = \sum_{k=1}^{N} \dot{\gamma}_k \mathbf{m}_k, \quad \mathbf{m}_k = \hat{\mathbf{b}}_k \otimes \hat{\mathbf{n}}_k \tag{7}$$

where $\mathbf{m}_k$ are the $k$th dyadic slip products of unit vectors $\hat{\mathbf{b}}_k$in the slip direction and $\hat{\mathbf{n}}_k$normal to the slip plane, and $\dot{\gamma}_k$ the shear rates on these systems. The specific constitutive functions for the plastic shearing rates $\dot{\gamma}_k$ on the slip systems are taken as

$$\dot{\gamma}_k = \dot{\gamma}_0 \left| \frac{\tau_k}{\tau_{k,\mathbf{crit}}} \right|^{1/\mathrm{m}} \mathrm{sgn}(\tau_k) \tag{8}$$

where $\tau_k$ is the resolved shear stress for the slip system $k$, and $\tau_{k,\mathrm{crit}}$ is the actual critical shear stress on the $k$th slip system. $\dot{\gamma}_0$ and $m$ are material parameters representing shearing rate and the rate sensitivity of slip. The calculation of $\tau_{k,\mathrm{crit}}$ has been achieved by accounting for latent hardening through the use of an appropriate hardening matrix,

$$\dot{\tau}_{k,\mathbf{crit}} = \sum_i h^{ki} |\dot{\gamma}|, \quad h^{ki} = q^{ki} h^{(i)} \tag{9}$$

where $h^{ki}$ is the rate of strain hardening on $k$th slip system due to a shearing on $i$th slip system, $q^{ki}$ is the hardening matrix describing the latent hardening behavior of a crystallite, and $h^{(i)}$ is the hardening rate of the single slip system $i$. In the present study, 12 slip systems with crystallographic $<110>$ slip directions and $\{111\}$ slip planes are taken into account for room temperature simulations of plastic deformation of aluminum. The matrix $h^{ki}$ can be taken as

$$h^{ki} = \begin{bmatrix} A & qA & qA & qA \\ qA & A & qA & qA \\ qA & qA & A & qA \\ qA & qA & qA & A \end{bmatrix} \tag{10}$$

where $q$ is the ratio of the latent hardening rate to the self-hardening rate, and $A$ is a $3 \times 3$ matrix populated by ones. Using this constitutive description renders the finite element method an elegant tool for detailed simulation studies of texture evolution and strain distribution under realistic boundary conditions. Each integration point can represent one orientation or map a larger set of crystals as outlined above.

### *4.2. Set-up for the finite element simulations of grain interaction and in-grain subdivision*

A finite element model was formulated to evaluate the influence of grain interaction on texture evolution as well as on in-grain subdivision. As shown in Fig. 1, 936 three-dimensional linear type elements (C3D8) were used in the model. Each element represents one individual grain with an identical initial crystal orientation everywhere in the element. The 936 different orientations are distributed randomly in orientation space. The orientations were statistically assigned to the elements so that they constitute a random artificial starting texture according to the starting conditions used for the experiments. Each element contains 8 integration points. All integration points in the same element have the same crystallographic orientation prior to loading but they can undergo different reorientation paths during straining. The subdivision of each grain into a set of initial orientations was used to predict the dependence of subdivision within individual initially uniform grains during loading the sample into the plastic regime. Coun-

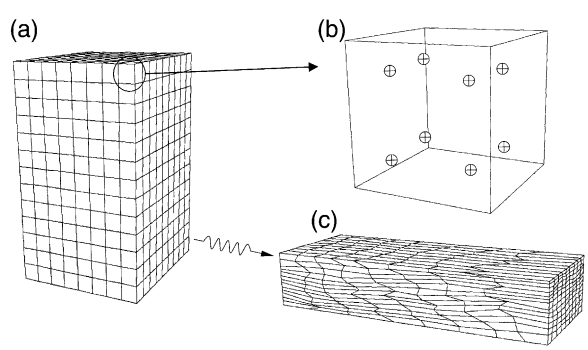


Fig. 1. FEM model setup for evaluating the influence of neighboring grains on the deformation texture. (a) 936 three-dimensional linear type elements were used. Each element represents one individual grain with one initial orientation. (b) Each element contains 8 integration points. (c) The boundary conditions preserved an ideal plane strain shape of the entire sample during forming.

ting all individual integration points a set of 7488 ($936 \times 8$) individual orientation points was used in the finite element simulation. An implicit crystal plasticity procedure proposed by Kalidindi et al. [35] was implemented and used for the time integration of the constitutive equations (see Section 4.1). Calculations were carried out using the finite element program ABAQUS in conjunction with the user defined material subroutine UMAT [36]. Simulations were based on $12 \times 1/\sqrt{3}\{1\underline{1}1\}^T$ $1/\sqrt{2} < 110 >^T$ slip systems using viscoplastic hardening. The model was used to simulate plane strain compression to 95% engineering thickness reduction (corresponding to a logarithmic strain of $\varepsilon = 3.0$). The orientation distribution functions were calculated from the orientations of all 7488 integration points by using spherical Gaussians with a scatter width of 5°.

### *4.3. Set-up for the finite element simulations without grain interaction and without in-grain subdivision*

A second crystal plasticity finite element simulation was conducted in order to obtain a deformation texture without any effects of the grain neighborhood. In this approach, only one element was used and 936 orientations were assigned to this element on the basis of the Taylor-type assumption given by Eq. (1).

### *4.4. Set-up for the finite element simulations of global texture variation as a function of grain interaction and in-grain subdivision*

A third set of finite element simulations was performed for obtaining an upper bound evaluation of the influence of changes in the grain neighborhood on the global texture evolution and on in-grain subdivision. For this purpose the 936 texture components were randomly assigned to the elements of the finite element mesh. By repeating this procedure 9 times, thereby giving each grain in each of the 9 subsequent simulation runs a different neighborhood configuration, we generated a data set which gives an overview of the spread in response of each texture component to a variety of neighborhood constraints. The results were statistically analyzed using the concept of a mean orientation [5,6]. The aim of this simulation series consisted in the identification of the maximum possible texture and subdivision variation which can be generated due to changes in the grain neighborhood. Further details are as described in Section 4.2.

### *4.5. Set-up for the homogenization simulation of texture as a function of grain interaction*

We selected four polycrystal homogenization models in order to compare their predictions with the experimental data and with the crystal plasticity finite element calculations, namely, the original no-strain-constraints (NC)-Sachs model, a modified grain interaction Sachs model suggested by Mao [37], the original full constraints (FC)-Taylor model and a modified Taylor grain interaction model by Schmitter [29,31]. For all predictions we used as a starting point a set of 936 individual orientations which were distributed homogeneously in orientation space. This set formed the random starting texture for all polycrystal homogenization simulations. All individual orientation changes were calculated in small strain steps of $\Delta\varepsilon = 0.01$ (logarithmic strain in sheet normal direction). The resulting deformation textures of the calculation at $\varepsilon = 3.0$ (corresponding to 95% engineering thickness reduction) were analyzed in the same way as the experiments and the crystal plasticity finite element predictions.

## 5. Results and discussion

### *5.1. Influence of grain neighborhood on global polycrystal texture*

Fig. 2(a) shows an experimental deformation texture obtained from a fine grained aluminum polycrystal with random starting texture after 95% cold rolling reduction (engineering strain). The texture is given in the reduced Euler space using contour lines for the orientation density in sections along the $\varphi_2$-axis in $\Delta\varphi_2 = 5°$ steps. The experimental texture is characterized by a weak incomplete $\alpha$-fiber consisting of a minor Goss component

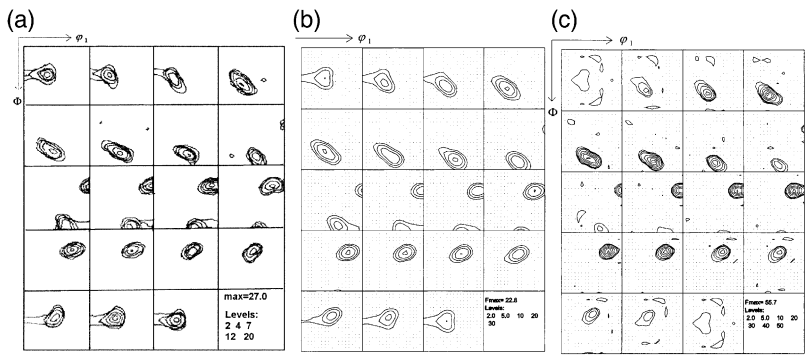


Fig. 2. (a) Rolling texture with random starting texture after 95% thickness reduction. (b,c) Deformation textures (95%) calculated by the crystal plasticity finite element method with different mesh configurations: (b) 936 elements were used to present the whole sample and each element represents one individual grain. (c) Only one element was used, but 936 orientations were assigned to the same integration point using the Taylor assumption.

and a strong Brass component with a maximum at $\varphi_1 = 30°$ (Fig. 3a) as well as a pronounced β-skeleton line (Fig. 3b) containing the Copper, S-, and Brass components (the Brass orientation occurs on both texture fibers, due to symmetry). The variable coordinates of the β-skeleton line in Euler space are given in Fig. 3(c).

Fig. 2(b) and 2(c) show the results for two crystal plasticity finite element simulations with different mesh configurations as outlined in Sections 4.2 and 4.3. Fig. 2(b) shows the simulation with 936 finite elements, where each element represents a different grain and contains 8 integration points with identical crystal orientation prior to loading. Fig. 2c shows a simulation with only one element where all 936 orientations, assembling the random starting texture, were mapped on the same integration point using the Taylor assumption. Qualitatively, the two simulations reproduce the most important features of the experimental texture, i.e. the presence of the Copper, S-, and Brass components (Figs. 2a and 3a-c). However, the simulation with 936 different elements which automatically takes into account grain interaction (Fig. 2b) reveals a much better agreement with the experimental texture (Fig. 2a). This applies particularly for the shape and orientation density of the incomplete α-fiber with a weak Goss and a pronounced Brass component as well as for the orientation density of the components on the β-skeleton line. The

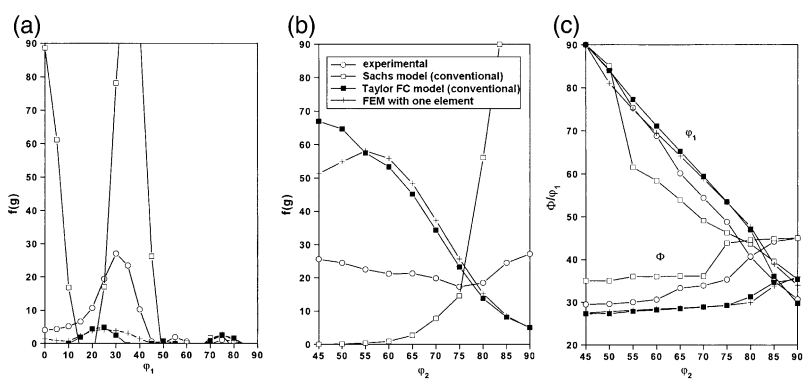


Fig. 3. Texture comparison of 95% cold-rolled aluminum sheet (○), no-strain-rate-constraints (NC) Sachs model (□), full-constraints (FC) Taylor model (■) and crystal plasticity finite element model with one element containing 936 orientations (+). (a) α-fiber, (b) β-skeleton line, (c) coordinates of β-skeleton line.

finite element simulation where only one element is used to map all 936 orientations via the Taylor assumption (Fig. 2c) predicts a deformation texture with a missing Goss component and strongly overemphasized Copper- and S-components on the β-skeleton line. The fiber analysis (Fig. 3) underlines that the disregard of grain interaction in the finite element simulation (when using only one element, Fig. 2c) leads to results which are almost identical to the predictions of the FC Taylor model. Fig. 3(b) shows particularly the abnormally high orientation density (≈60–70) near the Copper orientation ($\varphi_1 = 90°$, $\Phi = 30°$, $\varphi_2 = 45°$), while the orientation density of the Brass component ($\varphi_1 = 35°$, $\Phi = 45°$, $\varphi_2 = 0°$) is much lower than obtained by experiment. In contrast to this result, the NC–Sachs model shows the opposite tendency. Dropping the assumption of strain rate compatibility leads to an even worse correspondence between simulation and experiment (Fig. 3). Although both, the Taylor FC and the Sachs NC models do obviously not correspond to the experimental data, the Taylor constraint of strain rate compatibility among the grains seems to be more dominant for the evolution of the global texture than the Sachs constraint of force equilibrium at the grain boundaries. Similar arguments as for the Taylor FC model also apply for the finite element simulation with only one element. The comparison of the two classical homogenization models with the experiment and with the finite element prediction shown in Fig. 2(b) underlines that an improvement in texture prediction requires the incorporation of grain interaction.

Fig. 4 compares the results of the modified Sachs model [37], the Taylor-grain interaction model by Schmitter [29,31], and the crystal plasticity finite element model with 936 elements, i.e. with explicit consideration of the grain-neighbor configuration. All these texture predictions show a much better qualitative and quantitative agreement with the experimental results than the classical homogenization approaches presented in Fig. 3.

The α-fiber and the coordinates of the β-skeleton line (Figs. 4a and 4c) reveal that the Taylor grain interaction model predicts a slightly shifted Brass component ($\varphi_1 = 25°$, $\Phi = 45°$, $\varphi_2 = 0°$) when compared to the experimental data ($\varphi_1 = 30°$, $\Phi = 45°$, $\varphi_2 = 0°$). The modified Sachs approach also shows a slightly shifted Brass component with a maximum at $\varphi_1 = 35°$. The modified Taylor model underestimates the Goss orientation. The modified Sachs model reveals a better match for Goss. The crystal plasticity finite element model with 936 elements shows an excellent agreement with the experimentally observed position of the Brass component on the α-fiber, but the predicted orientation density is much below that observed in experiment. The results shown on the β-skeleton line (Fig. 4b) and on the β-skeleton line coordinates (Fig. 4c) also reveal a good qualitative correspondence to the experiments. While the modified Taylor grain interaction model reveals similar component positions though slightly sharper orientation density of the Copper and S components, the modified Sachs model overemphasizes both, the Copper and the S-orientation and underestimates the Brass-component. The crystal plasticity finite element model shows a good agreement for the Copper- and the S-orientations, but deviates for the Brass component.

Similar observations, in particular about the Brass component, were made earlier by Fortunier and Driver [5], Hirsch and Lücke [34], and Beaudoin et al. [38]. These studies showed that the development of the Brass, Copper, and S texture components is promoted by the relaxation of certain grain-to-grain shear constraints. Specifically, the exact position and intensity of the brass component depends on the micromechanical relaxation of the shear between rolling and transverse direction. This shear component was often not properly included in earlier simulations of channel die compression or rolling which were typically idealized by a (two dimensional) plane strain tensor. Fortunier and Driver [5], Hirsch and Lücke [34], and Beaudoin et al. [38] showed that the incorporation of additional kinematic degrees of freedom through inclusion of the out-of-plane dimension in certain Taylor-type models and finite element models leads to a more pronounced Brass texture.

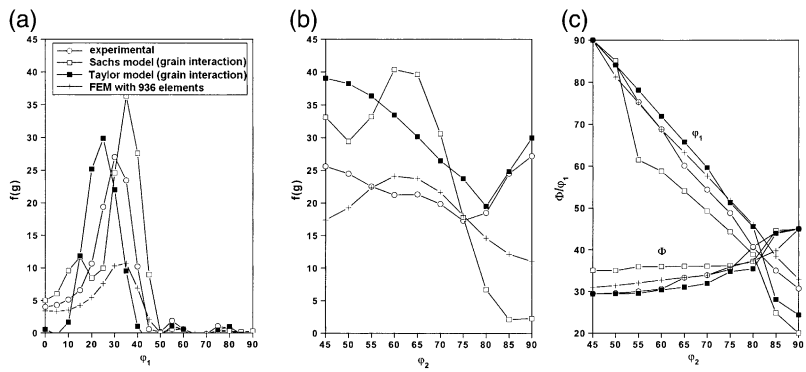


Fig. 4. Texture comparison of 95% cold-rolled aluminum sheet (○), modified Sachs model (□), modified Taylor grain interaction model (■), and crystal plasticity finite element model with 936 elements, each containing a set of 8 integration points with identical initial orientation (+). (a) α-fiber, (b) β-skeleton line, (c) coordinates of β-skeleton line.

### *5.2. Upper bound evaluation of the influence of grain neighborhood on the global texture evolution*

Fig. 5 shows a set of 9 simulation results which were obtained by randomly re-arranging the initial grain orientations assigned to the elements. This approach was originally introduced by Mika and Dawson [39] who used it to investigate the dependence of grain micromechanics on the local grain neighborhood. Employing a hybrid crystal plasticity finite element formulation these authors conducted a series of numerical experiments on the same set of crystals. Each simulation used a different spatial mapping of orientations to effectively alter the neighborhood of each crystal, allowing the dependence of deformation on crystal orientation to be examined.

In this study we conducted similar simulations using the crystal plasticity finite element model with 936 elements and 8 integration points in each element as explained in Section 4.2. The 9 different set-ups lead to 9 polycrystal configurations with different neighbor relationships among the grains. Comparing the predictions to the experimental results reveals three essential points. The first point is that the correspondence between the finite element model and the experimentally observed texture is qualitatively satisfying, but some quantitative and even qualitative deviations remain. For instance the predicted orientation density of the Brass component (Fig. 5a,b) is in all 9 simulations

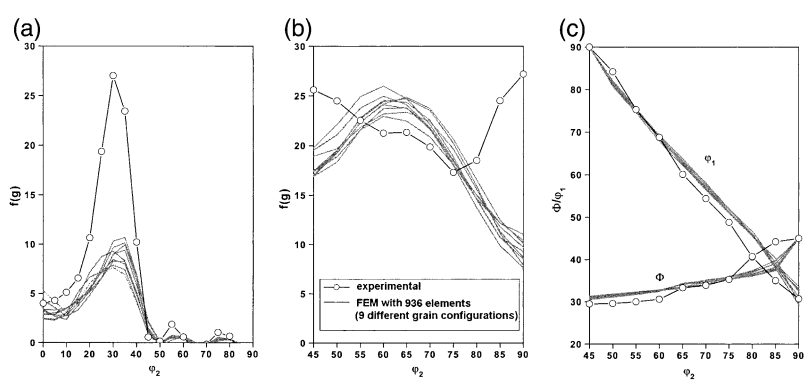


Fig. 5. Set of 9 crystal plasticity finite element simulations conducted by statistically varying the arrangement of the grains in a polycrystalline aggregate. Each grain is represented by 8 integration points and has different neighbor grains in each simulation. (a) α-fiber, (b) β-skeleton line, (c) coordinates of β-skeleton line.

much below the experimental value. Furthermore, the crystal plasticity finite element model pronounces the Copper-component somewhat less than the experiment. The correspondence of the exact positions of the occurring texture components in Euler space is excellent between experiment and simulation. The second point is that the 9 finite element simulations with their different grain configurations reveal excellent qualitative agreement with each other and only little variation in terms of the overall orientation density. All predictions occur within a similar spread of the overall orientation distribution. Sampling the results for the different neighborhood configurations shows that the upper bound for the variation of texture due to changes in grain interaction amounts at most to 5% in terms of the positions of the main texture components. In terms of the overall orientation density all predictions fall within a narrow orientation tube with an orientation scatter of 10% (β-fiber) to 20% (Brass component, α-fiber). This means that the influence of details of the grain neighborhood on the global texture evolution varies within these rather narrow bounds. The micromechanical analysis by Mika and Dawson presented in [39,40], however, suggests that the texture scatter is also dependent on the shape of the used finite elements. For instance in [40] Mika and Dawson used a polycrystal model which was constructed of 1099 rhombic dodecahedron shaped crystals, each discretized with 48 tetrahedra elements. The rhombic dodecahedron is a 12-sided, space-filling polyhedron and serves as an idealized crystal geometry. The scatter of the mean strain component in compression direction as a function of the Taylor factor extracted from simulations with different grain neighborhood was larger for rhombic dodecahedron shaped elements than for brick shaped elements [see Fig. 5 in 40]. Similar aspects associated with the element shape were discussed also in [39].

The third point that can be extracted from Fig. 5 is that all occurring texture components reveal similar scatter. In other words the texture systematically broadens into a texture tube with a scatter radius of 10–20% of the orientation density. When expressed in absolute values, the texture scatter among the 9 simulations is even more homogeneous with an average magnitude of $\Delta f(g)$ of about 2–3 for the main texture components. This indicates that the stability of all predicted texture components shows a similar dependence on changes in the grain neighbor configuration. At the same time, the positions of the main texture components are practically not affected by changes in the grain neighborhood configuration (see coordinates in Fig. 5c).

The simulations underline that the consideration of grain interaction has a clear influence on the global texture evolution of polycrystalline aluminum. Without reasonable consideration of this effect neither classical homogenization theory nor the crystal plasticity finite element simulations which map larger sets of orientations on one single integration point can predict textures accurately. It is an essential result that—since the individual textures fall within a common texture tube (Fig. 5)—the complex interaction of the grains with their neighbors may be tackled in a statistical fashion. This means that the input of the precise neighborhood topology of the grains, as randomly varied in the finite element simulations given in Fig. 5, has rather little qualitative effect on the final global texture. The simulations reveal that the orientation spread as a function of the exact grain neighborhood amounts at most to a variation in orientation density of 10% for the β-fiber components and 20% for the α-fiber components. The exact location of the texture components is even less affected by the fine details of the grain neighborhood arrangement.

This analysis of the finite element simulations corresponds to the simulation results obtained by the modified Taylor-type [29,31] and Sachs-type [37] models which also showed reasonable accuracy when compared to the finite element simulations and to the experiments. Considering the expense in computation time, these models are obviously more effective than finite element approaches. This means that modified homogenization models which contain plausible statistical assumptions on grain interaction should provide similar reliability as finite element simulations as far as the global texture prediction is concerned. This is particularly important for tackling plastic anisotropy on an engineering scale. Of course,

more detailed mechanisms of polycrystal plasticity can only be obtained via the finite element method, as will be discussed in the ensuing section.

### *5.3. Influence of grain interaction on in-grain subdivision*

During plastic deformation initially uniform grains do as a rule not rotate as units but subdivide into portions with a range of different orientations. This phenomenon which leads to the formation of in-grain orientation spreads does not only occur in the trivial case of externally imposed strain gradients but also under gradient-free external loadings. The intrinsic tendency (i.e. the orientation dependence) of grains to build up in-grain orientation gradients was recently systematically investigated using experiment, homogenization theory, and finite element simulations [10,39–43]. It was found in these studies that first, the formation of in-grain subdivision is strongly dependent on the initial orientation of the undeformed grain and that second, the formation of in-grain orientation gradients was less dependent on the details of the configuration of the neighbor grains.

Beaudoin et al. [42] were the first to address the problem of in-grain orientation subdivision in a very detailed fashion. In their work they showed that large orientation spreads which contained most orientation components from the β texture fiber can build up in plane strain deformed S-oriented grains.

Mika and Dawson [39] conducted crystal plasticity finite element simulations using rhombic dodecahedral-shaped crystals, each finely discretized with tetrahedral elements. They observed spatial in-grain variations in deformation even under simple external loadings leading to orientational grain subdivision phenomena. Particular attention in their study was focused on the resulting crystallographic misorientation across the newly formed boundaries and their orientations relative to the applied loads. This evolving in-grain boundary texture was compared to published experimental data obtained using TEM and Kikuchi pattern analysis.

In a second paper Mika and Dawson [40] investigated the deformations of a face-centered cubic polycrystal under idealized plane strain rolling conditions. The polycrystal model consisted of 1099 rhombic dodecahedron shaped crystals, each discretized with 48 tetrahedra elements. Different simulations used a different spatial mapping of orientations to effectively alter the neighborhood of each crystal, allowing the dependence of deformation on crystal orientation to be examined. The authors stated that coarse crystal discretizations are adequate for modeling bulk anisotropic properties, but a detailed investigation of local neighborhood effects require a finely discretized mesh that is better able to capture gradients in the deformation field.

Raabe et al. [43] have recently conducted an experimental and simulation study on the in-grain strain- and orientation gradients occurring in a coarse grained plane strain compressed aluminum polycrystal.

The crystal plasticity finite element simulations with 936 finite elements where each element contains 8 integration points conducted in our current study allow us to investigate the dependence of in-grain orientation subdivision as a function of changes in the grain neighbor configuration and to compare the results with homogenization theory. Since each of the 9 simulations was conducted with a different neighborhood arrangement differences in the subdivision behavior can be analyzed for each texture component as a function of the grain neighborhood.

For obtaining a quantitative description of the in-grain orientation scatter observed for the different grain neighborhoods we adopted the concept of mean orientation which was recently suggested by Delannay et al. [41]. As schematically shown in Fig. 6, the mean orientation in a set of discrete orientations is defined as the lattice orientation that has the minimum misorientation to all other orientations constituting the set.

Fig. 7 exemplary shows the subdivision results for one orientation out of the set of 936 different texture components. The {111} pole figure projection shows the orientational subdivision obtained after 95% thickness reduction (engineering strain) in the crystal plasticity finite element model for one particular starting orientation (indicated by the solid circle ●). The different neighborhood configurations were achieved by changing the arrange-

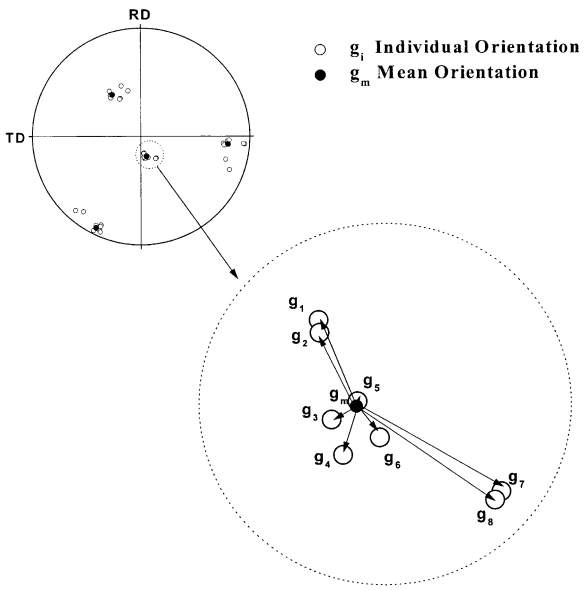


Fig. 6. The mean orientation (●) is defined as the lattice orientation which has the minimum misorientations to all orientations constituting a set of discrete orientations (○).

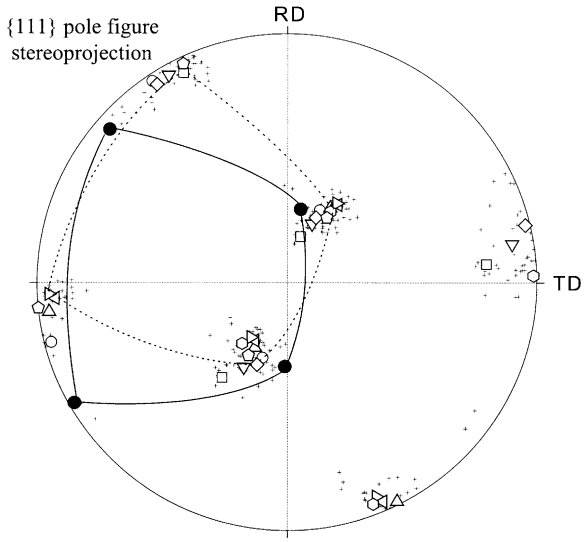


Fig. 7. One orientation from the set of 936 initial grain orientations showing the subdivision after a thickness reduction of 95% in the finite element model. Different neighborhood configurations were realized by changing the arrangement of the elements 9 times. The solid circle (●) represents the initial orientation and the open symbols (□○△▽...) represent the final mean orientations of the subdivided grains having different grain neighborhoods. Each element contained 8 initially identical orientation points. Therefore, in total 72 ($8 \times 9$) cross marks (+) are plotted to show the scatter in the orientational subdivision of the deformed grains.

ment of the starting orientations assigned to the finite elements 9 times. The 9 different final mean orientations obtained from each of those simulations with different grain neighborhood are represented by open symbols (∇△○□...). Each grain was represented by 8 integration points so that in total 72 ($8 \times 9$) cross marks (+) show the orientation fragments for each of the mean orientations as a scatter field of the deformed grains in the different surroundings. It can be seen that for the presented starting orientation (●) the different grain neighborhood led to different final mean orientations. All final mean orientations fall into a range of about 20° mutual orientation deviation. However, the main tendency of the reorientation of the original crystal reveals the same direction in orientation space. As will be discussed in the following, the orientation scatter observed in Fig. 7 is not necessarily typical of all strained grains since the effect is strongly orientation dependent. The example, however, shows that the misorientation between each mean orientation (obtained for one of the 9 finite element simulations) and the single orientations of each of the 8 integration points used for deriving the mean orientation can serve as a measure for the orientation scatter within the deformed grain.

Fig. 8 presents three of the 9 in-grain misorientation functions between the mean orientation and the orientations of the 8 integration points initially pertaining to the same grain. By using spherical Gaussians all misorientation results for the 936 different elements (grains) were mapped into Euler space according to their initial orientation position. The misorientation functions given in Fig. 8 is normalized so that the contour lines indicate not the absolute but the relative tendency of individual grains to build up in-grain orientation scatter. The procedure was repeated 9 times for the 9 different arrangements of the grain neighborhood. Fig. 8 shows only three of them, representing the upper and lower bounds as well as an example between them. It can be seen that different initial grain orientations reveal a different tendency to undergo orientational subdivision during plastic straining.

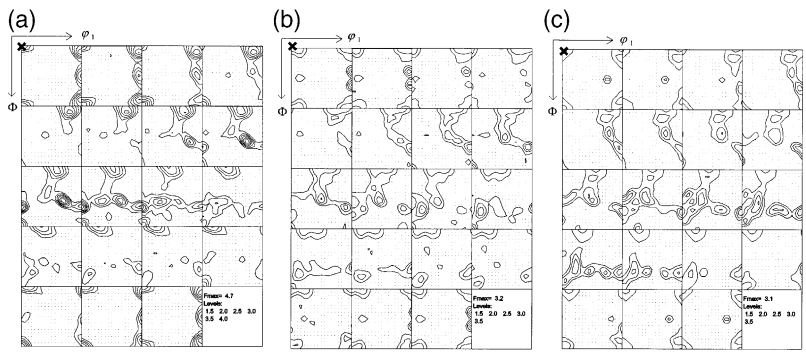


Fig. 8. In-grain misorientation functions between the mean orientation and the orientations of the 8 integration points initially pertaining to the same grain (element). The misorientation results for the 936 different elements were mapped according to their initial orientation position. The contour lines indicate not the absolute but the relative tendency of individual grains to build up in-grain orientation scatter. The procedure was repeated 9 times for the 9 different arrangements of the grain neighborhood (only 3 representative results are shown).

Although the intensity distribution is different in the three simulated in-grain misorientation distribution functions, the basic tendency, i.e. the orientation dependence to undergo orientation subdivision is rather similar in the three results.

As is known from numerous previous investigations, the cube orientation ($\varphi_1 = 0°$, $\Phi = 0°$, $\varphi_2 = 0°$, and $\varphi_1 = 90°$, $\Phi = 0°$, $\varphi_2 = 0°$, marked by **x** in Fig. 8c) has in fcc metals a strong tendency to undergo orientation subdivision both, in polycrystals [40–43] as well as in single crystals [44,45]. The calculations also show that the cube orientation keeps its tendency to subdivide in different neighborhood configurations. The different sections containing the cube orientations in Euler space reveal further different scatter tendencies in the three different rotation directions. A different behavior can be found for the 90° about the sheet normal rotated Goss component ($\varphi_1 = 90°$, $\Phi = 45°$, $\varphi_2 = 0°$). Fig. 8(a) shows a strong in-grain-subdivision for this component while Fig. 8(c) shows no tendency to subdivide. This means that this texture component (which does not play an important role in aluminum rolling textures) shows substantial sensitivity with respect to its neighboring grain configuration. A strong maximum in the normalized in-grain misorientation distribution can be observed for a component about 10° off the Copper orientation. The main texture components on the β-skeleton line, i.e. the Copper, S-, and Brass orientations reveal a very small tendency to undergo orientation subdivision according to our finite element simulations. This observation was also experimentally confirmed by the work of Delannay et al. [41]. The qualitative similarity in the orientation dependence of the in-grain misorientation function among the different finite element simulations for most of the orientations suggests the conclusion that the basic inclination of a grain to undergo orientation subdivision is strongly determined by its initial orientation and the basic constraints (intrinsic dependence) and less determined by the details of the neighborhood configuration (extrinsic dependence).

### *5.4. Limitation of the analysis*

The application of the crystal plasticity finite element model with 936 elements allows one to conduct detailed calculations about the influence of the neighbor grains on the individual deformation behavior of different crystals as well as on the global texture evolution of polycrystals. However, several limitations of this method should be emphasized.

First, the grain shape assumed in the simulations has a simple brick-like geometry. More accurate simulations of grain subdivision should take into account the real topology of the grains and use more elements in one individual grain. Second, in the present work we used a random initial texture in the experiments and a set of 963 discrete crystal-

lographic orientations which formed a random initial texture in the simulations. However, real polycrystalline materials rarely have a random texture. This means we cannot exclude that the presence of pronounced starting textures might influence the statistics of the grain neighborhood configuration, rendering randomly chosen single grain mechanics a cluster-mechanical phenomenon, where larger sets of similarly oriented neighboring crystals undergo cooperative shape changes. Such phenomena are well known from ridging and roping phenomena.

## 6. Conclusions

We investigated the dependence of crystallographic deformation textures and in-grain subdivision phenomena in aluminum polycrystals on grain interaction. We used experiments, homogenization theory, and crystal plasticity finite element methods. The main conclusions are:

- Grain neighborhood interaction has a significant influence on the evolution of the global deformation texture. Quantitative predictions of deformation textures, be it with homogenization or crystal plasticity finite element theory, cannot be obtained without taking the influence of grain interaction into account.
- The influence of the grain neighborhood on the global texture evolution can be described by statistics. Crystal plasticity finite element simulations with different grain neighborhood configurations predicted slightly different textures which all fall in a narrow orientation tube with an orientation scatter between 10% (β-fiber) to 20% (Brass component, α-fiber) in terms of the orientation density and only 5% in terms of orientation changes. Correspondingly modified Taylor-type and Sachs-type models, therefore, in principle represent effective and fast methods to capture this systematic influence into polycrystal modeling.
- The tendency of grains to undergo orientation subdivision during straining is much stronger affected by their initial orientation (intrinsic dependence) rather than by the details of the grain neighborhood surrounding them (extrinsic dependence). Statistical variations in the grain neighborhood revealed mostly a similar orientation dependence of orientational subdivision, but the magnitude of the effect varied.

## References

[1] Barrett CS, Levenson LH. Trans. Metall. Soc. AIME 1940;137:112.
[2] Essmann U, Rapp M, Wilken M. Acta Metall 1968;16:1275.
[3] Barlow CYJ, Bay B, Hansen N. Phil. Mag 1985;51:253.
[4] Skalli A, Fortunier R, Driver JH. Acta Metall 1985;33:997.
[5] Fortunier R, Driver JH. Acta Metall 1987;35:1335.
[6] Akef A, Driver JH. Mat. Sci. Eng. 1991;A132:245.
[7] Raabe D. Phys. Stat. Sol. (b) 1994;181:291.
[8] Raabe D. Steel Research 1995;66:222.
[9] Boeslau J, Raabe D. Materials Science Forum 1994;501:157–62.
[10] Raabe D, Zhao Z, Park S-J, Roters F. Acta Mater 2002;50:421.
[11] van Houtte P. In: Wenk H-R, editor. Preferred Orientations in Deformed Metals and Rocks. An Introduction of Modern Texture Analysis. New York: Academic Press; 1985.
[12] Aernoudt E, van Houtte P, Leffers T. In: Mughrabi H, editor. Deformation and Textures of Metals at Large Strain. Calm RW, Haasen P, Kramer EJ editors. Plastic Deformation and Fracture of Materials of Materials Science and Technology—A Comprehensive Treatment, 6. Weinheim: VCH; 1993. Chapter 3.
[13] Hosford WF. The mechanics of crystals and textured polycrystals. Oxford: Oxford University Press, 1993.
[14] Kocks UF, Tóme CN, Wenk H-R. Texture and anisotropy. Cambridge: Cambridge University Press, 1998.
[15] Raabe D. Computational materials science. Weinheim: Wiley-VCH, 1998.
[16] Taylor GI. J. Inst. Metals 1938;61:307.
[17] Bishop JFW, Hill R. Phil. Mag 1951;42:414.
[18] Sachs G. Z. Ver. Dtsch. Ing. 1928;72-22:734.
[19] Eshelby JD. Proc. R. Soc. London 1957;A241:376.
[20] Kröner E. Z. Phys 1958;151:504.
[21] Kröner E. Acta Metall 1961;9:155.
[22] Bunge H-J. Kristall u. Technik 1970;5:145 (in German).
[23] Barlat F, Lian J. Int. J. Plast 1989;5:51.
[24] Van Houtte P, Mols K, Van Bael B, Aernoudt E. Textures Microstructures 1989;11:23.
[25] Van Bael A, Van Houtte P, Aernoudt E, Hall FR, Pillinger I, Hartley P, Sturgess CEN. Textures Microstructures 1991;14-18:1007.
[26] Aretz H, Luce R, Wolske M, Kopp R, Goerdeler M, Marx V, Pomana G, Gottstein G. Model. Simul. Mater. Sc. Eng 2000;8:881.

[27] Beckers B, Sebald R, Pomana G, Gade D, Gottstein, G. In: Carstensen JV, Leffers T, Lorentzen T, Pedersen OB, Sorensen BF, Winther G. Proc. 19th RISO Intern. Symp. on Materials Science: Modelling of Structure and Mechanics of Materials from Microscale to Product, Roskilde, Denmark: RISO Nat. Lab., 1998. p. 219.
[28] Wagner P. Ph. D. Thesis, RWTH Aachen, Germany, 1994.
[29] Schmitter U. Diplomarbeit RWTH Aachen, Germany, 1992.
[30] Van Houtte P, Delannay L, Samajdar I. Textures Microstructures 1999;31:109.
[31] Raabe D. Acta Metall 1995;43:1023.
[32] Humphreys FJ, Hatherly M. Recrystallization and related annealing phenomena. Oxford: Pergamon Press, 1995.
[33] Sarma GB, Dawson PR. Intern. J. Plast. 1023;1996:12.
[34] Hirsch J, Lücke K. Acta Metall 1988, 36, 2863 and 2883.
[35] Kalidindi SR, Bronkhorst CA, Anand L, Mech J. Phys. Solids 1992;40:537.
[36] ABAQUS/Standard User's Manual, Volume II, 14.1.4-1, Hibbitt, Karlsson and Sorensen, Pawtucket, RI, 1999.
[37] Mao W. Mater. Sci. Eng. 1998;A257:171.
[38] Beaudoin A, Dawson PR, Mathur KK, Kocks UF. Int. J. Plast 1995;11:501.
[39] Mika DP, Dawson PR. Acta Mater 1999;47:1355.
[40] Mika DP, Dawson PR. Mater. Sc. Eng. 1998;A257:62.
[41] Delannay L, Mishin OV, Juul Jensen D, Van Houtte P. Acta Mater 2001;49:2441.
[42] Beaudoin A, Mecking H, Kocks UF. Philos. Mag. 1996;A73:1503.
[43] Raabe D, Sachtleber M, Zhao Z, Roters F, Zaefferer S. Acta Mater 2001;49:3433.
[44] Wert JA, Liu Q, Hansen N. Acta Metall 1996;45:2565.
[45] Basson F, Driver JH. Acta Metall 2000;48:2101.